

Denudation systematics inferred from in situ cosmogenic 10Be concentrations in fine (50-100 μm) and medium (100-250 μm) sediments of the Var River basin, southern French Alps

Apolline Mariotti, Pierre-Henri Blard, Julien Charreau, Carole Petit, Stéphane Molliex, D.L. Bourles

▶ **To cite this version:**

Apolline Mariotti, Pierre-Henri Blard, Julien Charreau, Carole Petit, Stéphane Molliex, et al.. Denudation systematics inferred from in situ cosmogenic 10Be concentrations in fine (50-100 μm) and medium (100-250 μm) sediments of the Var River basin, southern French Alps. Earth Surface Dynamics, 2019, 7 (4), pp.1059-1074. 10.5194/esurf-7-1059-2019 . hal-02377519

HAL Id: hal-02377519
https://hal.science/hal-02377519

Submitted on 23 Nov 2019

HAL is a multi-disciplinary open access archive for the deposit and dissemination of scientific research documents, whether they are published or not. The documents may come from teaching and research institutions in France or abroad, or from public or private research centers.

L'archive ouverte pluridisciplinaire **HAL**, est destinée au dépôt et à la diffusion de documents scientifiques de niveau recherche, publiés ou non, émanant des établissements d'enseignement et de recherche français ou étrangers, des laboratoires publics ou privés.

https://doi.org/10.5194/esurf-2019-37
Preprint. Discussion started: 1 August 2019
© Author(s) 2019. CC BY 4.0 License.



Earth Surface Dynamics Discussions
Open Access
EGU

Denudation systematics inferred from in situ cosmogenic ^{10}Be concentrations in fine (50–100 µm) and medium (100–250 µm) sediments of the Var River basin, southern French Alps

Apolline Mariotti[1], Pierre-Henri Blard[1], Julien Charreau[1], Carole Petit[2], Stéphane Molliex[3, 1], ASTER Team[4]

[1]CRPG, CNRS - Université de Lorraine, UMR 7358, 54500 Vandoeuvre-lès-Nancy, France
[2]Geoazur, Université de Nice, 06905 Sophia Antipolis, France
[3]Laboratoire Géosciences Océan, Institut Universitaire Européen de la Mer, 29280 Plouzané, France
[4]CEREGE, Laboratoire LN2C, CNRS Université Aix Marseille, 13090 Aix-en-Provence, France

Correspondence to: Apolline Mariotti (apolline.mariotti@univ-lorraine.fr)

https://doi.org/10.5194/esurf-2019-37
Preprint. Discussion started: 1 August 2019
© Author(s) 2019. CC BY 4.0 License.



Earth Surface Dynamics Discussions
Open Access
EGU

Abstract

Marine sedimentary archives are well dated and often span several glacial cycles; cosmogenic ^{10}Be concentrations in their detrital quartz grains could thus offer the opportunity to reconstruct a wealth of past denudation rates. However, these archives often comprise sediments much finer (<250 µm) than typically analyzed in ^{10}Be studies, and few studies have measured ^{10}Be concentrations in quartz grains smaller than 100 µm or assessed the impacts of mixing, grain size and interannual variability on the ^{10}Be concentrations of such fine-grained sediments. Here, we analyzed the in situ cosmogenic ^{10}Be concentrations of quartz grains in the 50–100 and 100–250 µm size fractions of sediments from the Var basin (southern French Alps) to test the reliability of denudation rates derived from ^{10}Be analyses of fine sands. The Var basin has a short transfer zone and highly variable morphology, climate and geology, and we test the impact of these parameters on the observed ^{10}Be concentrations. Both analyzed size fractions returned similar ^{10}Be concentrations in downstream locations, notably at the Var's outlet, where concentrations ranged from $(4.02 \pm 0.78) \times 10^4$ to $(4.40 \pm 0.64) \times 10^4$ atoms g_{quartz}^{-1}. By comparing expected and observed ^{10}Be concentrations at three major river junctions, we interpret that sediment mixing is efficient throughout the Var basin. We resampled four key locations one year later, and despite variable climatic parameters during that period, interannual ^{10}Be concentrations were in agreement within uncertainties, except for one upper subbasin. The ^{10}Be-derived denudation rates of Var subbasins range from 0.10 ± 0.01 mm yr^{-1} to 0.57 ± 0.09 mm yr^{-1}, and spatial variations are primarily controlled by the average subbasin slope. The integrated denudation rate of the entire Var basin is 0.24 ± 0.04 mm yr^{-1}, in agreement with other methods. Our results demonstrate that fine-grained sediments (50–250 µm) return accurate denudation rates and are thus suitable targets for future ^{10}Be applications, such as studies of paleo-denudation rates using offshore sediments.

https://doi.org/10.5194/esurf-2019-37
Preprint. Discussion started: 1 August 2019
© Author(s) 2019. CC BY 4.0 License.



Earth Surface Dynamics Discussions
Open Access
EGU

1 Introduction

Understanding landscape dynamics and denudation processes is crucial for human activities: for example, soil formation rates (Heimsath et al., 1997; Stockmann et al., 2014) control agricultural resources (Montgomery, 2007) whereas landslide occurrences (Hovius and Stark, 2007; Yu et al., 2019) are key to managing natural hazards (Kirschbaum et al., 2010). Denudation is the combined effect of physical erosion and chemical weathering processes, and may vary with time. Because climate exerts a strong control on denudation (Molnar, 2004; Peizhen et al., 2001; Yanites and Ehlers, 2012), it is important to predict how landscapes will respond to the large and rapid climate changes expected in the future. Terrestrial cosmogenic nuclides (TCNs) in river sediments provide a means to determine denudation rates at the basin scale (Bierman and Steig, 1996; Brown et al., 1995; Granger et al., 1996; von Blanckenburg, 2005). Thus, for decades, TCN (mostly ^{10}Be) concentrations have been measured in present and past river sediments across a wide variety of climatic and geological contexts to quantify denudation rates (see review by Portenga and Bierman, 2011) over different time scales (Bekaddour et al., 2014; Charreau et al., 2011; Granger and Schaller, 2014; Grischott et al., 2016, 2017; Marshall et al., 2017; Puchol et al., 2016; Schaller et al., 2002). However, although offshore marine sedimentary archives are well dated and often record several glacial cycles, they have remained unused for reconstruction of paleo-denudation rates, mainly because their grain sizes are too fine to facilitate standard in situ ^{10}Be analyses in quartz. Indeed, typical cosmogenic dating samples have grain sizes of 250 µm to 1 mm. In deep (>200 m water depth) marine environments, sediments of such grain sizes are restricted to submarine canyons in which the stratigraphic record is poorly preserved. Thus, analyzing TCNs in fine sand fractions (50–100 µm) is prerequisite to reconstructing past denudation rates from marine sediments because this granulometric range often dominates in offshore, turbidite-rich sedimentary cores (Bonneau et al., 2014; Jorry et al., 2011).

Furthermore, grain size distributions are not always uniform across continental basins (Lukens et al., 2016), and ^{10}Be concentrations in fine sands and silts at river outlets may not be representative of their entire drainage area. Stochastic hillslope processes (e.g. landslides) can also introduce grain size perturbations (Attal et al., 2015) and thus may affect TCN concentrations and associated interpretations (Puchol et al., 2014; Brown et al., 1995). Several studies have suggested that sediment mixing is not always efficient in mountainous environments (Binnie et al., 2006; Savi et al., 2014), which would further bias interpreted denudation rates. Finally, ^{10}Be concentrations integrate the denudation signal over time periods dependent on the denudation rate that correspond to the time needed to erode 60 cm of rock (Lal, 1991). Perturbations in the sedimentary routing process, such as human-induced erosion or stochastic events like landslides or flash floods, can potentially affect ^{10}Be concentrations over much shorter time scales and therefore bias the interannual consistency of the ^{10}Be signal (Dingle et al., 2018; Lupker et al., 2012; Sosa Gonzalez et al., 2017).

The effects of spatial mixing, grain size and temporal variability on TCN concentrations have mostly been tested on sand fractions coarser than 125 µm. With the exception of Brown et al. (1995, 1998), who investigated grain sizes as small as 63 µm, these processes remain largely unexplored in fine size fractions <125 µm. Therefore, it is critical to understand how fine sediments capture denudation rates in onshore basins and if these processes alter the observed TCN concentrations.

Here, we measured in situ ^{10}Be concentrations in the 50–100 and 100–250 µm size fractions of modern quartz sediments of the Var River. The Var drains a mountainous basin in the southern French Alps, is characterized by a steep mean slope of 23°, and its small alluvial plain limits sediment storage (Bonneau et al., 2017). The Var sedimentary system responds quickly (i.e. within 1000 yr) to climatic forcings, and is thus an ideal setting to test the suitability of fine-grained sediments to record paleo-denudation rates (Bonneau et al., 2017). We analyzed multiple samples within the Var basin to assess the spatial variability of denudation rates across a high diversity of geomorphic and climatic contexts. We then traced the

https://doi.org/10.5194/esurf-2019-37
Preprint. Discussion started: 1 August 2019
© Author(s) 2019. CC BY 4.0 License.



Earth Surface Dynamics Discussions
Open Access
EGU

upstream to downstream evolution of ^{10}Be concentrations in both analyzed size fractions to monitor the impact of grain size on the observed ^{10}Be concentration, the sediment mixing efficiency at major fluvial junctions, and the interannual variability of the denudation signal.

2 The Var basin

The Var and its main tributaries (Vésubie, Tinée, Estéron and Coulomp Rivers) drain a mountainous basin of 2800 km^2 in the southern French Alps (Fig. 1). This steep basin is characterized by a mean slope of 23° and elevations ranging from 0 to 3143 m above sea level with a mean elevation of 1200 m (Fig. 1). The Var basin can be divided into two main geological regions: crystalline basement in the north and sedimentary terrains in the south. In the northern and highest part of the basin, the Mercantour-Argentera Massif comprises migmatites, gneiss and granite (Fig. 1) inherited from the Paleozoic Hercynian orogen (El Bedoui et al., 2011). The late Paleozoic to Cenozoic sedimentary cover of the southern and western parts of the basin mainly comprises Mesozoic marls and limestones (Kerckhove and Montjuvent, 1977; Roure et al., 1976). These sediments also include Permian pelites and sandstones (locally overlain by Cenozoic marls, limestones and sandstones) at the southern edge of the Mercantour-Argentera Massif and in the inner part of the Var basin (Fig. 1). In the southernmost part of the basin, the Pliocene to Quaternary Gilbert delta developed after sea level rise in the Mediterranean Sea following the Messinian salinity crisis (Mulder et al., 1996).

Stochastic erosional processes such as landslides – the most studied being La Clapière landslide in the Tinée valley (El Bedoui et al., 2009; Casson et al., 2003) – and screes occur in the steepest part of the basin (Julian, 1977). Four hydropower dams have been built in the upper part of the basin (Fig. 1), but only the Lac Long dam (2500 m elevation) has a significant water storage capacity (4 700 000 m^3). Nine sedimentary dams were built in the lowest part of the basin in the 1970s to enhance sediment deposition and protect the city of Nice (Anthony and Julian, 1999). The climate in the Var basin is mostly controlled by elevation and is thus highly variable, from a Mediterranean climate in the south to a mountainous climate in the north. Between 1981 and 2010, the mean annual temperature and mean annual precipitation recorded at Nice (2 m above sea level; Fig. 1) were 16 °C and 733 mm yr^{-1}, respectively, and those at Guillaumes (790 m above sea level; Fig. 1) were 10.7 °C and 910 mm yr^{-1}, respectively (Meteo France database; https://donneespubliques.meteofrance.fr).

3 Methods and results

3.1 Calculation of denudation rates

In situ cosmogenic ^{10}Be is produced by cosmic rays in minerals such as quartz within the uppermost layer of Earth's surface (Lal and Peters, 1967). The ^{10}Be concentration in quartz depends directly on the time spent near the surface and, thus, on the denudation rate (Lal, 1991). Therefore, the average denudation rate at the basin scale can be derived from the ^{10}Be concentrations measured in detrital quartz exported by fluvial sediments and sampled at the outlet of the studied basin (Brown et al., 1995). Assuming that denudation is steady-state and the ^{10}Be decay constant is negligible (von Blanckenburg, 2005), the spatially averaged denudation rate of a basin is inversely proportional to the ^{10}Be concentration in sediments (Brown et al., 1995; Granger et al., 1996). The basin-averaged denudation rate can thus be calculated as:

$$\bar{\varepsilon} = \sum_{i,x} \frac{\bar{P}_i \ \Lambda_i}{\rho \ \bar{C}}, \quad (1)$$

where i refers to the different ^{10}Be production pathways and associated particles (n for neutron, μs for slow muons and μf for fast muons). $\bar{P}_i$ are the mean basin-wide ^{10}Be production rates, computed from the arithmetic mean of spallogenic and muogenic production using specific scalings for each production pathway as a function of elevation and latitude: P_n = 4.11 ± 0.19 atoms g^{-1} yr^{-1}, $P_{\mu s}$ = 0.011 ± 0.001 atoms g^{-1} yr^{-1} and $P_{\mu f}$ = 0.039 ± 0.004 atoms g^{-1} yr^{-1} (Braucher et al., 2011; Martin

https://doi.org/10.5194/esurf-2019-37
Preprint. Discussion started: 1 August 2019
© Author(s) 2019. CC BY 4.0 License.



Earth Surface Dynamics Discussions
Open Access
EGU

et al., 2017). Λ_i are the attenuation lengths for each particle: Λ_n = 160 g cm^{-2}, $\Lambda_{\mu s}$ = 1500 g cm^{-2} and $\Lambda_{\mu f}$ = 4320 g cm^{-2} (Braucher et al., 2011). Finally, ρ is the mean density of the eroded material (2.7 g cm^{-3}) and $\bar{C}$ is the ^{10}Be concentration measured in the fluvial sediments collected at the basin outlet.

We calculated basin-averaged ^{10}Be production rates for each production pathway and each studied subbasin using the Basinga GIS tool (Charreau et al., 2019), based on the Lal–Stone time-dependent scaling model (Lal, 1991; Nishiizumi et al., 1989; Stone, 2000), and using up-to-date worldwide production rates computed by the Cosmic Ray Exposure program online calculator (https://crep.otelo.univ-lorraine.fr/; Martin et al., 2017). We accounted for basin topography using a cell-by-cell approach based on the 5 m resolution digital elevation model "RGE ALTI" produced by the French Institut National de l'Information Géographique et Forestière. Denudation rates were corrected for paleomagnetic variations that occurred during the integration time and topographic shielding (Charreau et al., 2019). Topographic shielding factors were calculated using the ArcGIS toolbox of Codilean (2006), which computes both self-shielding and shading. Quartz-free areas were excluded from the basin-averaged production rate calculations based on 1:50 000 and 1:250 000 scale French Geological Survey geological maps (Bigot et al., 1967; Campredon et al., 1980; Faure-Muret et al., 1954, 1957; Gèze et al., 1969; Ginsburg et al., 1980; Kerckhove and Montjuvent, 1977; Kerckhove and Roux, 1976; Kerckhove and Thouvenot, 2010; Roure et al., 1976). Quartz-bearing zones comprise 730 km^2, corresponding to 26 % of the total surface area of the Var basin. We calculated denudation rates for each of the Var's subbasins using the measured ^{10}Be concentrations and Eq. (1) (Table 1). We also calculated effective denudation rates and ^{10}Be concentrations in the downstream part of three basins by correcting for the contribution of upstream nested subbasins (Table 2, Fig. S1) (see Granger et al., 1996 and Portenga et al., 2015 for methods).

3.2 Sampling and ^{10}Be analyses

We collected eleven sediment samples (2 kg each) from active riverbeds of the Var River and its main tributaries (Vésubie, Tinée, Estéron and Coulomp Rivers) in November 2016. Sampling locations were carefully selected to avoid any human-induced perturbations in the basin, such as dams (Fig. 1). The Tinée and Vésubie Rivers were each sampled at two locations: one within the crystalline massif (TIN-16-2 and VES-16-1) and one just upstream of their junctions with the Var River (TIN-16-1 and VES-16-2) (Fig. 1). The Coulomp and Estéron Rivers were each sampled upstream of their junctions with the Var River (COU-16-1 and EST-16-1). The Var River was sampled at five locations throughout the basin: one upstream of the Tinée confluence (VAR-16-2), one upstream of the Vésubie confluence (VAR-16-3), one upstream of the Estéron confluence (VAR-16-4) and two at the river outlet near the Mediterranean Sea (VAR-16-5A and VAR-16-5B). In November 2017, we resampled three of the rivers in four of the same locations: VAR-17-2, VAR-17-5B, VES-17-1 and TIN-17-2.

We sieved the samples to obtain 50–100 and 100–250 µm grain size fractions. Quartz grains were isolated from both fractions by magnetic separation and successive HCl + H_2SiF_6 baths. The pure quartz grains were then leached three times in HF to dissolve 30 % of the total weight of quartz and eliminate meteoric ^{10}Be contamination (Brown et al., 1991). We then spiked the purified quartz samples with 0.3 mg of the Centre de Recherches Pétrographiques et Géochimiques (CRPG) ^{9}Be carrier solution (concentration of 2020 ± 83 ppm, corresponding to ~2.25 × 10^9 atoms ^{9}Be). The spiked quartz samples were then completely dissolved in 48 % HF; beryllium was separated using anion and cation exchange columns and pH-sensitive precipitations before being oxidized to BeO, mixed with Nb powder and loaded into targets for measurement of ^{10}Be/^{9}Be ratios using the ASTER accelerator mass spectrometer at Centre Européen de Recherche et d'Enseignement des Géosciences de l'Environment (CEREGE).

https://doi.org/10.5194/esurf-2019-37
Preprint. Discussion started: 1 August 2019
© Author(s) 2019. CC BY 4.0 License.



All measured $^{10}Be/^{9}Be$ ratios were calibrated using the CEREGE STD11 in-house normalization, which is similar to the KNSTD07 normalization and assumes a $^{10}Be/^{9}Be$ ratio of $(2.79 \pm 0.03) \times 10^{-11}$ for the SRM4325 standard material (Braucher et al., 2015). Five and three chemical blanks were processed and measured during the 2016 and 2017 analytical sessions, respectively; the 2016 and 2017 blanks yielded $^{10}Be/^{9}Be$ ratios of $(2.05 \pm 0.38) \times 10^{-15}$ and $(1.99 \pm 0.43) \times 10^{-15}$, respectively.

3.3 Results

The raw ^{10}Be concentrations of the sediment samples are reported in Supplementary Data. Blank-corrected ^{10}Be concentrations are reported in Table 1 and summarized in Figure 2 for the 2016 sampling. We obtained twenty ^{10}Be measurements from the eleven samples collected in 2016; concentrations were measured in both the 50–100 and 100–250 µm grain size fractions for all samples except VAR-16-4 and TIN-16-2, which did not yield sufficient amounts of quartz in the 50–100 µm fraction. We obtained five ^{10}Be measurements from the four samples collected in 2017; both grain size fractions were measured for VAR-17-2, only the 50–100 µm fraction was measured for VAR-17-5B and only the 100–250 µm fraction was measured for VES-17-1 and TIN-17-2. Measurement blanks accounted for, on average, 11 ± 7 % of the measured $^{10}Be/^{9}Be$ ratios. Most samples had similar ^{10}Be concentrations within uncertainties for the 50–100 and 100–250 µm grain size fractions (Table 1 and Fig. 2). VES-16-1 and VES-16-2 are two exceptions because they yielded different ^{10}Be concentrations in each size fraction: for both samples, the 50–100 µm fraction had higher ^{10}Be concentrations than the 100–250 µm fraction. Importantly, the most distal samples collected at the outlet of the Var River (VAR-16-5A and VAR-16-5B) had undistinguishable ^{10}Be concentrations in both size fractions, ranging from $(4.02 \pm 0.78) \times 10^{4}$ atoms g^{-1} to $(4.40 \pm 0.64) \times 10^{4}$ atoms g^{-1}. Sediments resampled in 2017 (VAR-17-2, VAR-17-5B, VES-17-1 and TIN-17-2) had concentrations similar within uncertainties to the 2016 samples (Table 1); only the 50–100 µm fraction of VAR-17-2 had a significantly lower ^{10}Be concentration compared to the same size fraction of the 2016 sample.

Calculated denudation rates for 2016 ranged from 0.10 ± 0.01 mm yr^{-1} (Coulomp River, COU-16-1, 100–250 µm) to 0.57 ± 0.09 mm yr^{-1} (Vésubie River, VES-16-1, 100–250 µm) (Fig. 3). The averaged denudation rates calculated at the outlet of the Var basin were 0.24 ± 0.03 and 0.25 ± 0.04 mm yr^{-1} for the 100–250 and 50–100 µm fractions, respectively. For the 2017 samples, denudation rates ranged from 0.17 ± 0.05 mm yr^{-1} (Var River, VAR-17-2, 100–250 µm) to 0.52 ± 0.06 mm yr^{-1} (Vésubie River, VES-17-1, 100–250 µm), and the average denudation rate at the Var outlet was 0.27 ± 0.04 mm yr^{-1} for the 50–100 µm fraction.

The integration time of the ^{10}Be signal deduced from each sample varied from 1 kyr (Vésubie River, VES-16-1, 100–250 µm) to 6 kyr (Coulomp River, COU-16-1, 100–250 µm) (Table 1).

4 Discussion

4.1 Comparison of ^{10}Be-derived denudation rates with the modern sediment flux

To validate the use of ^{10}Be-derived denudation rates obtained from fine-grained sediments, we compare the denudation rates obtained at the outlet of the Var River (samples VAR-16-5A and VAR-16-5B) to previous results for the Var basin. Both the denudation rates derived from the 100–250 µm (0.24 ± 0.03 mm yr^{-1}) and 50–100 µm fractions (0.25 ± 0.04 mm yr^{-1}) at the Var outlet are in remarkable agreement with the denudation rate of 0.22 mm yr^{-1} calculated by Bonneau et al. (2017) based on modern Var River sediment fluxes estimated by Mulder et al. (1996). This demonstrates that fine-grained sediments can

https://doi.org/10.5194/esurf-2019-37
Preprint. Discussion started: 1 August 2019
© Author(s) 2019. CC BY 4.0 License.



Earth Surface Dynamics Discussions
Open Access
EGU

accurately preserve and transport the ^{10}Be-derived denudation signal across the Var basin. Furthermore, because the ^{10}Be-derived denudation rate was calculated solely for quartz-bearing rocks whereas the sediment flux-based estimate includes all lithologies, the agreement between the two methods suggests that quartz-bearing rocks are eroded at the same rate as other rock types in the basin. We note that the integration time of the ^{10}Be signal at the outlet (VAR-16-5A and VAR-16-5B) is between 2.3 and 2.6 kyr (Table 1), whereas the modern sediment flux was estimated over a 20 year period (between 1974 and 1994; Mulder et al., 1996). The agreement of the two methods thus suggests that denudation rates in the Var basin have been stable over the last 2.6 kyr.

4.2 Comparison with previously published ^{10}Be studies across the Alps

In this subsection, we compare the Var basin denudation rates with other studies reporting ^{10}Be-derived denudation rates in similar environments of the Alps. It is notably important to verify that the variability of the ^{10}Be signal carried by fine-grained sediments follows the same trend as larger grain sizes. Multiples studies have explored the relationship between denudation and landscape parameters such as topography and climate at a global scale (e.g. Portenga and Bierman, 2011) and at the scale of the Alps (Delunel et al., 2010; Dixon et al., 2016; Molliex et al., 2016; Norton et al., 2011; Wittmann et al., 2007). The two most frequent parameters used in correlation with denudation rates are the average slope (Dixon et al., 2016; Portenga and Bierman, 2011; Wittmann et al., 2007) and average elevation of the basin (Delunel et al., 2010; Molliex et al., 2016; Wittmann et al., 2007). Figure 4 compares the ^{10}Be-derived denudation rates of each subbasin with its mean slope and elevation. We calculated subbasin effective denudation rates by excluding nested upstream subbasins for three subbasins (VAR-16-2, TIN-16-1 and VES-16-2) following the method of Portenga et al. (2015) (Table 2) to account for the local parameters of each subbasin. Furthermore, Figure 4 compares our data from the Var basin with previously published ^{10}Be-derived denudation rates across the Alps, as available in the OCTOPUS Database (Codilean et al., 2018). We selected 133 basins with drainage areas comparable to the Var basin and its subbasins, i.e. ranging from 10 to 10 000 km^2 (Fig. 4). Alpine denudation rates range from 0.01 ± 0.01 mm yr^{-1} (Buechi et al., 2014) to 2.83 ± 0.93 mm yr^{-1} (Norton et al., 2010) for grain sizes ranging from 63 to 1000 μm, consistent with the overall variability of denudation rates across the Var basin (Fig. 4).

In Figure 4, we classified ^{10}Be-derived denudation rates for the Alps into three granulometric groups: <250, 250–500 and >500 μm, and we note several key observations. First, the maximum grain size analyzed does not seem to induce a strong control on the ^{10}Be-derived denudation rates at the scale of the Alpine belt. Second, the mean slope of the basin does not exert a linear control on denudation rates because the highest denudation rates are not observed on the steepest slopes (Fig 4. a); denudation rates on average slopes of 23–32° are characterized by the highest average values, but are highly variable. In the Var basin, denudation rates increase nonlinearly with subbasin slope, as observed in mountainous basins elsewhere (Binnie et al., 2007; Dixon et al., 2016; Montgomery and Brandon, 2002; Roering et al., 2001; Wittmann et al., 2007). This nonlinear relationship has been interpreted as the result of a change from diffusive to non-diffusive transport dynamics above a given slope angle, variously reported to be between 22° and 30° (Binnie et al., 2007; Montgomery and Brandon, 2002; Roering et al., 2001). This slope threshold is about 30° in the Var basin. On average slopes of 16–30°, denudation rates in the Var basin are rather restricted, from 0.10 ± 0.01 mm yr^{-1} (COU-16-1, 100–250 μm) to 0.22 ± 0.04 mm yr^{-1} (VAR-16-2, 100–250 μm). Denudation rates increase on the steepest average slopes (>30°), with values ranging from 0.20 ± 0.04 mm yr^{-1} (VES-16-2, 50–100 μm) to 0.83 ± 0.28 mm yr^{-1} (TIN-16-1, 100–250 μm) (Table 2; Fig. S1). The hillslope transport model of Montgomery and Brandon (2002), based on the model of Roering et al. (1999), can explain the nonlinear relationship between average slope and denudation rate observed in our data (Fig. 4a). Third, it has been shown that elevation exerts a positive control on denudation rates across the Alps (Fig. 4b), either due to frost cracking (Delunel et al., 2010), the impact of U-shaped glacial morphologies (Molliex et al., 2016) or greater uplift rates in higher regions (Wittmann et al., 2007). In

https://doi.org/10.5194/esurf-2019-37
Preprint. Discussion started: 1 August 2019
© Author(s) 2019. CC BY 4.0 License.



the Var basin, the relationship between elevation and denudation appears rather weak, notably because the Tinée subbasin (sample TIN-16-1, 100–250 μm) presents the highest denudation rate (0.83 ± 0.28 mm yr^{-1}) although situated at a relatively low elevation (1486 m). The high denudation rate in this area is most likely the result of the steep average slope (~32°) (Table 2; Fig. 4; Fig. S1). In the Alps, slope and elevation display a nearly linear relationship for slopes lower than ~20°, but the two variables are much more scattered for slopes steeper than 25° (Fig. 4c).

Overall, the ^{10}Be-derived denudation rates we obtained from fine-grained sediments (50–250 μm) in the Var basin are in the range of previously reported rates in the Alps. Our rates are also similar to those inferred from a wide range of grain sizes (63–1000 μm) at various slopes and elevations. This result suggests that denudation rates derived from ^{10}Be concentrations in fine-grained sediments (50–250 μm) properly record denudation in this region, with slope being the dominant control on denudation rates. This conclusion is further supported by the similar ^{10}Be concentrations of the 50–100 and 100–250 μm size fractions throughout the basin, the notable exception being the steep upstream Vésubie subbasin (VES-16-1, Fig. 5), discussed in Sect. 4.3.

4.3 Impact of grain size on ^{10}Be concentrations

In the Vésubie subbasin, the ^{10}Be concentrations of the two size fractions did not overlap within uncertainties (Table 1; Fig. 5). To understand this discrepancy, we investigated the potential controls of topographic and climatic parameters on the ^{10}Be concentrations of the sediments (Fig 5). For basins with nested upstream subbasins (VAR-16-2 and VES-16-2), we calculated subbasin ^{10}Be concentrations by removing the contribution of their upstream subbasins (COU-16-1 and VES-16-1, respectively; Table 2, Fig. S1). It is thus apparent that above 2000 m elevation in the upper Vésubie (VES-16-1), sediments of the 50–100 μm size fraction have significantly higher ^{10}Be concentrations than those in the 100–250 μm fraction, whereas the two fractions have relatively similar concentrations in the downstream subbasin (VES-16-2; Fig. 5a). Because mean annual temperature is a function of elevation, it is tempting to propose that the main control on this discrepancy is climatic (Fig. 5b). A plausible temperature-altitude control could be related to frost cracking, an erosion mechanism enhanced by cold conditions. Indeed, in the nearby Ecrins Pelvoux massif (~120 km north of the Var basin), Delunel et al. (2010) found a positive correlation between elevation and ^{10}Be-derived denudation rates.

An alternative possibility is that the slope of the subbasin affects the contributions of different grain sizes to the observed ^{10}Be concentration (Fig. 5c). Steeper areas are characterized by a larger contribution of sediments from deep-seated landslides, which are typically coarser sediments (Attal et al., 2015) with lower ^{10}Be concentrations (Puchol et al., 2014). The mixing of landslide-derived material with finer hillslope surficial sediments will thus produce sediments with different ^{10}Be concentrations in the fine and coarse fractions (Fig. 5c). Additional data are necessary to distinguish between the effects of climate and landslides in generating the observed discrepancy between the 50–100 and 100–250 μm fractions in the upper Vésubie subbasin. However, we stress that this grain size effect is limited to the Vésubie upstream subbasin and is not observed in larger subbasins below 2000 m elevation. Importantly, we observe no effect of grain size on the measured ^{10}Be concentrations at the outlet of the Var basin (Fig. 2).

4.4 Sediment mixing

To determine if the ^{10}Be concentrations measured at the river outlet are representative of the entire basin, it is critical to assess whether the sediments are well mixed throughout the basin (Bierman and Steig, 1996; Binnie et al., 2006). This is of increased importance in the Var basin due to the heterogeneous distribution of quartz-bearing rocks. Because the basin-averaged denudation rate integrates surfaces of variable denudation rates, the average rate will not reflect the correct repartition of source areas if sediment mixing is inefficient, leading to erroneous denudation rates. Therefore, we here

https://doi.org/10.5194/esurf-2019-37
Preprint. Discussion started: 1 August 2019
© Author(s) 2019. CC BY 4.0 License.



Earth Surface Dynamics Discussions
Open Access
EGU

investigate the efficiency of sediment mixing by calculating the expected ^{10}Be concentration of sediments downstream of a particular junction, C_{cal}, as the ^{10}Be concentration of sediments from each tributary weighted by the sedimentary fluxes upstream of the junction (Binnie et al., 2006; Clapp et al., 2002; Matmon et al., 2003; Neilson et al., 2017; Savi et al., 2014):

$$C_{\text{cal}} = \frac{C_1 \times A_1 \times \varepsilon_1 + C_2 \times A_2 \times \varepsilon_2}{A_1 \times \varepsilon_1 + A_2 \times \varepsilon_2}, \quad (2)$$

where subscripts 1 and 2 denote the two upstream subbasins, C_1 and C_2 are the ^{10}Be concentrations of their respective sediments measured upstream of the junction, ε_1 and ε_2 are their denudation rates, and A_1 and A_2 are the surface areas comprising quartz-bearing rocks in each subbasin. If sediment mixing is efficient, the calculated concentrations will be similar to that measured downstream of the junction.

We calculated mixed concentrations at the Var-Tinée (VAR-16-3, junction I), Var-Vésubie (VAR-16-4, junction II) and Var-Estéron junctions (VAR-16-5A/B, junction III) (Fig 6.). We used the ^{10}Be concentrations measured in both size fractions for junction I, but only those of the 100–250 µm fractions (the only available data) in junctions II and III. At junction I, the calculated ^{10}Be concentrations for both grain sizes are in agreement with the measured ^{10}Be concentrations. Similarly, at junction II, the expected and measured ^{10}Be concentrations are compatible within uncertainties. At junction III, the difference between the measured and expected ^{10}Be concentrations is greater, though they are compatible within uncertainties (C_{measured} = 4.07 ± 0.74 atoms g^{-1} vs C_{cal} = 3.55 ± 0.50 atoms g^{-1}). This discrepancy may be due to the 16 km distance between the Var-Estéron junction, where the mixed ^{10}Be concentration is computed, and the downstream sampling location, VAR-16-5A/B. Indeed, between these two points, the basin is developed over quartz-rich Pliocene conglomerates (Fig. 1) whose contribution may slightly modify the observed ^{10}Be concentrations. Finally, the presence of sedimentary dams in this area does not strongly affect the observed ^{10}Be concentrations of the sediments. Consequently, the fluvial dynamic of the Var basin efficiently mixes the sedimentary material transported by each major tributary.

4.5 Interannual variability of ^{10}Be concentrations

As in most mountainous areas, the discharge regimes of the Var River and its upstream tributaries (Tinée and Vésubie) are characterized by erratic and torrential behavior (Anthony and Julian, 1999). Therefore, it is important to assess whether extreme rainfall events, which are frequent in the study area (Anthony and Julian, 1999) and generate floods with high sedimentary loads (Mulder et al., 1996), affect the observed ^{10}Be concentrations. In November 2016, heavy rainfall induced multiple high discharge events in the Tinée, Vésubie and upstream Var (Fig. 7b). Consequently, the discharge at the outlet of the Var increased to over 200 m^3 s^{-1} seven days before sampling. Conversely, 2017 was characterized by more moderate rainfall and the discharge at the Var outlet was around 10 m^3 s^{-1} during sampling. Despite these differences, the ^{10}Be concentrations measured in 2016 and 2017 are in agreement (Fig. 7a), with the exception of the finer sediments (50–100 µm) in the upstream Var, which yielded statistically different ^{10}Be concentrations in 2016 and 2017 (samples VAR-16-2 and VAR-17-2). This difference may have resulted from a stochastic event (e.g. landslide) that locally modified the ^{10}Be concentrations. Such perturbations are rarely buffered in such a small subbasin (the VAR-2 subbasin has a quartz-bearing surface area of only 83.3 km^2) (Niemi et al., 2005; Yanites et al., 2009). However, upstream valleys (i.e. the Tinée and Vésubie) are the most subject to such events (Anthony and Julian, 1999), but do not show any interannual variations. Most importantly, the fine sediment (50–100 µm) samples at the Var outlet (VAR-16-5B and VAR-17-5B) were remarkably similar between the two years (Table 1, Fig. 7a). Thus, despite highly variable discharge and the occurrence of stochastic events, the integrated ^{10}Be concentrations of sediments exported by the entire Var basin are not affected by a detectable interannual variability.

https://doi.org/10.5194/esurf-2019-37
Preprint. Discussion started: 1 August 2019
© Author(s) 2019. CC BY 4.0 License.



Earth Surface Dynamics Discussions
Open Access
EGU

5 Conclusions

We documented modern denudation rates in the Var basin (southern French Alps) using ^{10}Be concentrations measured in quartz grains in the 50–100 and 100–250 μm size fractions of detrital river sediments. ^{10}Be-derived denudation rates range from 0.10 ± 0.01 mm yr^{-1} to 0.57 ± 0.09 mm yr^{-1} within the basin and the average denudation rate obtained at the Var outlet is 0.24 ± 0.04 mm yr^{-1}, in remarkable agreement with the denudation rate of 0.22 mm yr^{-1} determined based on the Var River sediment flux (Bonneau et al., 2017). The spatial variability of denudation rates within the Var basin is on the same order of magnitude as other ^{10}Be studies across the Alps. The dominant control on denudation rates in the Var basin appears to be the average slope of the subbasin, consistent with previous studies. The ^{10}Be concentrations of the two analyzed size fractions were different only in the upper and steeper parts of the basin, but were similar at the Var outlet. By comparing the expected and measured ^{10}Be concentrations at three tributary junctions, we demonstrated that sediment mixing is efficient throughout the basin. We investigated the interannual variability of ^{10}Be concentrations in sediments under different discharge regimes during wet and dry years (2016 and 2017, respectively); we observed local variations, but concentrations at the outlet were similar each year. Our results demonstrate that fine-grained sediments (50–250 μm) return denudation rates similar to those of coarser sediments typically used in ^{10}Be studies (250 μm to 1 mm) and are thus suitable targets for future ^{10}Be applications, such as studies of paleo-denudation rates using offshore sediments.

6 Data availability

A raw data table including all samples is available in supplement.

7 Authors contributions

AM, PHB and JC designed the study. AM, PHB, JC and CP collected the samples for analysis. AM prepared the samples for ^{10}Be analysis and the ASTER Team measured the ^{10}Be/^{9}Be ratios using the French Service National AMS ASTER. AM, PHB, JC and SM analyzed the data. AM wrote the initial manuscript and all authors commented and contributed to the final version.

8 Competing interests

Authors declare that they have no conflict of interest.

9 Acknowledgements

This research was funded by the ANR JC EroMed project (N° ANR-17-CE01-0011-01; Principal Investigator P.-H. Blard). This work is part of the PhD thesis of Apolline Mariotti, whose scholarship was jointly supported by the CNRS and the Région Grand Est. Fruitful discussions with Samuel Toucanne, Stephan Jorry, Lucille Bonneau and Vincent Godard benefited the design of the study and interpretation of the results. We are grateful to Emmanuel Davy and Abdellah Zitouni for their help with quartz separation at CRPG, and to Laëticia Léanni and Régis Braucher for their expertise in ^{10}Be wet chemistry at LN2C/CEREGE. Robert Dennen is acknowledged for proofreading and improving the overall readability of the manuscript.

https://doi.org/10.5194/esurf-2019-37
Preprint. Discussion started: 1 August 2019
© Author(s) 2019. CC BY 4.0 License.



References

Anthony, E. J. and Julian, M.: Source-to-sink sediment transfers, environmental engineering and hazard mitigation in the steep Var River catchment, French Riviera, southeastern France, Geomorphology, 31(1–4), 337–354, doi:10.1016/S0169-555X(99)00088-4, 1999.

Attal, M., Mudd, S. M., Hurst, M. D., Weinman, B., Yoo, K., and Naylor, M.: Impact of change in erosion rate and landscape steepness on hillslope and fluvial sediments grain size in the Feather River basin (Sierra Nevada, California), Earth Surf. Dyn., 3(1), 201–222, doi:10.5194/esurf-3-201-2015, 2015.

El Bedoui, S., Guglielmi, Y., Lebourg, T., and Pérez, J.-L.: Deep-seated failure propagation in a fractured rock slope over 10,000 years: The La Clapière slope, the south-eastern French Alps, Geomorphology, 105(3–4), 232–238, doi:10.1016/j.geomorph.2008.09.025, 2009.

El Bedoui, S., Bois, T., Jomard, H., Sanchez, G., Lebourg, T., Trics, E., Guglielmi, Y., Bouissou, S., Chemenda, A., Rolland, Y., Corsini, M., and Pérez, J. L.: Paraglacial gravitational deformations in the SW Alps: a review of field investigations, ^{10}Be cosmogenic dating and physical modelling, Geol. Soc. London, Spec. Publ., 351(1), 11–25, doi:10.1144/SP351.2, 2011.

Bekaddour, T., Schlunegger, F., Vogel, H., Delunel, R., Norton, K. P., Akçar, N., and Kubik, P. W.: Paleo erosion rates and climate shifts recorded by Quaternary cut-and-fill sequences in the Pisco valley, central Peru, Earth Planet. Sci. Lett., 390, 103–115, doi:10.1016/j.epsl.2013.12.048, 2014.

Bierman, P. R. and Steig, E. J.: Estimating rates of denudation using cosmogenic isotope abundances in sediment, Earth Surf. Process. Landforms, 21(2), 125–139, doi:10.1002/(SICI)1096-9837(199602)21:2<125::AID-ESP511>3.0.CO;2-8, 1996.

Bigot, M., Damiani, L., Dellery, B., Durozoy, G., Faure-Muret, A., and Fallot, P.: Carte géologique de la France à 1/50 000 - Saint Martin - Vésubie - Le Boréon, BRGM., 1967.

Binnie, S. A., Phillips, W. M., Summerfield, M. A., and Fifiled, K. L.: Sediment mixing and basin-wide cosmogenic nuclide analysis in rapidly eroding mountainous environments, Quat. Geochronol., 1(1), 4–14, doi:10.1016/j.quageo.2006.06.013, 2006.

Binnie, S. A., Phillips, W. M., Summerfield, M. A., and Fifiled, K. L.: Tectonic uplift, threshold hillslopes, and denudation rates in a developing mountain range, Geology, 35(8), 743, doi:10.1130/G23641A.1, 2007.

von Blanckenburg, F.: The control mechanisms of erosion and weathering at basin scale from cosmogenic nuclides in river sediment, Earth Planet. Sci. Lett., 237(3–4), 462–479, doi:10.1016/j.epsl.2005.06.030, 2005.

Bonneau, L., Jorry, S. J., Toucanne, S., Silva Jacinto, R., and Emmanuel, L.: Millennial-Scale Response of a Western Mediterranean River to Late Quaternary Climate Changes: A View from the Deep Sea, J. Geol., 122(6), 687–703, doi:10.1086/677844, 2014.

Bonneau, L., Toucanne, S., Bayon, G., Jorry, S. J., Emmanuel, L., and Silva Jacinto, R.: Glacial erosion dynamics in a small mountainous watershed (Southern French Alps): A source-to-sink approach, Earth Planet. Sci. Lett., 458, 366–379, doi:10.1016/j.epsl.2016.11.004, 2017.

Braucher, R., Merchel, S., Borgomano, J., and Bourlès, D. L.: Production of cosmogenic radionuclides at great depth: A multi element approach, Earth Planet. Sci. Lett., 309(1–2), 1–9, doi:10.1016/j.epsl.2011.06.036, 2011.

Braucher, R., Guillou, V., Bourlès, D. L., Arnold, M., Aumaître, G., Keddadouche, K., and Nottoli, E.: Preparation of ASTER in-house 10Be/9Be standard solutions, Nucl. Instruments Methods Phys. Res. Sect. B Beam Interact. with Mater. Atoms, 361, 335–340, doi:10.1016/j.nimb.2015.06.012, 2015.

Brown, E. T., Edmond, J. M., Raisbeck, G. M., Yiou, F., Kurz, M. D., and Brook, E. J.: Examination of surface exposure ages of Antarctic moraines using in situ produced 10Be and 26Al, Geochim. Cosmochim. Acta, 55(8), 2269–2283, doi:10.1016/0016-7037(91)90103-C, 1991.

https://doi.org/10.5194/esurf-2019-37
Preprint. Discussion started: 1 August 2019
© Author(s) 2019. CC BY 4.0 License.



Brown, E. T., Stallard, R. F., Larsen, M. C., Raisbeck, G. M., and Yiou, F.: Denudation rates determined from the accumulation of in situ-produced 10Be in the luquillo experimental forest, Puerto Rico, Earth Planet. Sci. Lett., 129(1–4), 193–202, doi:10.1016/0012-821X(94)00249-X, 1995.

Brown, E. T., Stallard, R. F., Larsen, M. C., Bourlès, D. L., Raisbeck, G. M., and Yiou, F.: Determination of predevelopment denudation rates of an agricultural watershed (Cayaguás River, Puerto Rico) using in-situ-produced 10Be in river-borne quartz, Earth Planet. Sci. Lett., 160(3–4), 723–728, doi:10.1016/S0012-821X(98)00123-X, 1998.

Buechi, M. W., Kober, F., Ivy-Ochs, S., Salcher, B. C., Kubik, P. W., and Christl, M.: Denudation rates of small transient catchments controlled by former glaciation: The Hörnli nunatak in the northeastern Swiss Alpine Foreland, Quat. Geochronol., 19, 135–147, doi:10.1016/j.quageo.2013.06.005, 2014.

Campredon, R., Aicard, P., Bambier, A., and Durozoy, G.: Carte géologique de la France à 1/50 000 - Entrevaux, BRGM., 1980.

Casson, B., Delacourt, C., Baratoux, D., and Allemand, P.: Seventeen years of the "La Clapière" landslide evolution analysed from ortho-rectified aerial photographs, Eng. Geol., 68(1–2), 123–139, doi:10.1016/S0013-7952(02)00201-6, 2003.

Charreau, J., Blard, P.-H., Puchol, N., Avouac, J.-P., Lallier-Vergès, E., Bourlès, D. L., Braucher, R., Gallaud, A., Finkel, R. C., Jolivet, M., Chen, Y., and Roy, P.: Paleo-erosion rates in Central Asia since 9 Ma: A transient increase at the onset of Quaternary glaciations?, Earth Planet. Sci. Lett., doi:10.1016/j.epsl.2011.01.018, 2011.

Charreau, J., Blard, P., Zumaque, J., Martin, L. C. P., Delobel, T., and Szafran, L.: BASINGA: a cell-by-cell GIS toolbox for computing BASIN averaGe scaling factors, cosmogenic production rates and denudation rAtes, Earth Surf. Process. Landforms, esp.4649, doi:10.1002/esp.4649, 2019.

Chittenden, H., Delunel, R., Schlunegger, F., Akçar, N., and Kubik, P. W.: The influence of bedrock orientation on the landscape evolution, surface morphology and denudation (10 Be) at the Niesen, Switzerland, Earth Surf. Process. Landforms, 39(9), 1153–1166, doi:10.1002/esp.3511, 2014.

Clapp, E. M., Bierman, P. R., and Caffee, M. W.: Using 10Be and 26Al to determine sediment generation rates and identify sediment source areas in an arid region drainage basin, Geomorphology, 45(1–2), 89–104, doi:10.1016/S0169-555X(01)00191-X, 2002.

Codilean, A. T.: Calculation of the cosmogenic nuclide production topographic shielding scaling factor for large areas using DEMs, Earth Surf. Process. Landforms, 31(6), 785–794, doi:10.1002/esp.1336, 2006.

Codilean, A. T., Munack, H., Cohen, T. J., Saktura, W. M., Gray, A., and Mudd, S. M.: OCTOPUS: An Open Cosmogenic Isotope and Luminescence Database, Earth Syst. Sci. Data Discuss., (March), 1–23, doi:10.5194/essd-2018-32, 2018.

Delunel, R., van der Beek, P. A., Carcaillet, J., Bourlès, D. L., and Valla, P. G.: Frost-cracking control on catchment denudation rates: Insights from in situ produced 10Be concentrations in stream sediments (Ecrins–Pelvoux massif, French Western Alps), Earth Planet. Sci. Lett., 293(1–2), 72–83, doi:10.1016/j.epsl.2010.02.020, 2010.

Dingle, E. H., Sinclair, H. D., Attal, M., Rodés, Á., and Singh, V.: Temporal variability in detrital 10Be concentrations in a large Himalayan catchment, Earth Surf. Dyn., 6(3), 611–635, doi:10.5194/esurf-6-611-2018, 2018.

Dixon, J. L., von Blanckenburg, F., Stüwe, K., and Christl, M.: Glaciation's topographic control on Holocene erosion at the eastern edge of the Alps, Earth Surf. Dyn., 4(4), 895–909, doi:10.5194/esurf-4-895-2016, 2016.

Donnini, M., Frondini, F., Probst, J.-L., Probst, A., Cardellini, C., Marchesini, I., and Guzzetti, F.: Chemical weathering and consumption of atmospheric carbon dioxide in the Alpine region, Glob. Planet. Change, 136, 65–81, doi:10.1016/j.gloplacha.2015.10.017, 2016.

Faure-Muret, A., Fallot, P., Bordet, P., Lemoine, M., and Raguin, E.: Carte géologique de la France à 1/50 000 - Saint Etienne de Tinée, BRGM., 1954.

Faure-Muret, A., Fallot, P., Carrive, J., Bordet, P., and Goquel, J.: Carte géologique de la France à 1/50 000 - Puget-Théniers., 1957.

https://doi.org/10.5194/esurf-2019-37
Preprint. Discussion started: 1 August 2019
© Author(s) 2019. CC BY 4.0 License.



Fick, S. E. and Hijmans, R. J.: WorldClim 2: new 1-km spatial resolution climate surfaces for global land areas, Int. J. Climatol., 37(12), 4302–4315, doi:10.1002/joc.5086, 2017.

Gèze, B., Lanteaume, M., Peyre, Y., and Vernet, J.: Carte géologique de la France à 1/50 000 - Menton-Nice, BRGM., 1969.

Ginsburg, L., Montenat, C., Baubron, J. and Alziar, G.: Carte géologique de la France à 1/50 000 - Roquesteron, BRGM., 1980.

Glotzbach, C., Van Der Beek, P. A., Carcaillet, J., and Delunel, R.: Deciphering the driving forces of erosion rates on millennial to million-year timescales in glacially impacted landscapes: An example from the Western Alps, J. Geophys. Res. Earth Surf., 118(3), 1491–1515, doi:10.1002/jgrf.20107, 2013.

Granger, D. E. and Schaller, M.: Cosmogenic nuclides and erosion at the watershed scale, Elements, 10(5), 369–373, doi:10.2113/gselements.10.5.369, 2014.

Granger, D. E., Kirchner, J. W., and Finkel, R. C.: Spatially Averaged Long-Term Erosion Rates Measured from in Situ-Produced Cosmogenic Nuclides in Alluvial Sediment, J. Geol., 104(3), 249–257, doi:10.1086/629823, 1996.

Grischott, R., Kober, F., Lupker, M., Hippe, K., Ivy-Ochs, S., Hajdas, I., Salcher, B. C., and Christl, M.: Constant denudation rates in a high alpine catchment for the last 6 kyrs, Earth Surf. Process. Landforms, doi:10.1002/esp.4070, 2016.

Grischott, R., Kober, F., Lupker, M., Reitner, J. M., Drescher-Schneider, R., Hajdas, I., Christl, M., and Willett, S. D.: Millennial scale variability of denudation rates for the last 15 kyr inferred from the detrital 10 Be record of Lake Stappitz in the Hohe Tauern massif, Austrian Alps, The Holocene, 27(12), 1914–1927, doi:10.1177/0959683617708451, 2017.

Heimsath, A. M., Dietrich, W. E., Nishiizumi, K., and Finkel, R. C.: The soil production function and landscape equilibrium, Nature, 388(6640), 358–361, doi:10.1038/41056, 1997.

Hovius, N. and Stark, C. P.: Landslide-driven erosion and topographic evolution of active mountain belts, in Landslides from Massive Rock Slope Failure, pp. 573–590, Springer Netherlands, Dordrecht., 2007.

Hurst, M. D., Mudd, S. M., Yoo, K., Attal, M., and Walcott, R.: Influence of lithology on hillslope morphology and response to tectonic forcing in the northern Sierra Nevada of California, J. Geophys. Res. Earth Surf., 118(2), 832–851, doi:10.1002/jgrf.20049, 2013.

Jorry, S. J., Jégou, I., Emmanuel, L., Silva Jacinto, R., and Savoye, B.: Turbiditic levee deposition in response to climate changes: The Var Sedimentary Ridge (Ligurian Sea), Mar. Geol., 279(1–4), 148–161, doi:10.1016/j.margeo.2010.10.021, 2011.

Julian, M.: Une carte géomorphologique des Alpes Maritimes franco-italiennes au 1/200 000e en couleurs. Présentation succincte, Méditerranée, 28(1), 45–53, doi:10.3406/medit.1977.1709, 1977.

Kerckhove, C. and Montjuvent, G.: Carte géologique de la France à 1/250 000 - Gap, BRGM., 1977.

Kerckhove, C. and Roux, M.: Carte géologique de la France à 1/50 000 - Castellane, BRGM., 1976.

Kerckhove, C. and Thouvenot, F.: Carte géologique de la France à 1/50 000 - Allos, BRGM., 2010.

Kirschbaum, D. B., Adler, R., Hong, Y., Hill, S., and Lerner-Lam, A.: A global landslide catalog for hazard applications: Method, results, and limitations, Nat. Hazards, 52(3), 561–575, doi:10.1007/s11069-009-9401-4, 2010.

Lal, D.: Cosmic ray labeling of erosion surfaces: in situ nuclide production rates and erosion models, Earth Planet. Sci. Lett. Elsevier Sci. Publ. B.V, 104, 424–439 [online] Available from: http://ac.els-cdn.com.bases-doc.univ-lorraine.fr/0012821X9190220C/1-s2.0-0012821X9190220C-main.pdf?_tid=49363256-6df1-11e7-a80d-00000aab0f6b&acdnat=1500627054_02968c28f830d18001b2130ecd5d29c6 (Accessed 21 July 2017), 1991.

Lal, D. and Peters, B.: Cosmic Ray Produced Radioactivity on the Earth, in Kosmische Strahlung II / Cosmic Rays II, vol. 9 / 46 / 2, edited by K. Sitte, pp. 551–612, Springer Berlin Heidelberg, Berlin, Heidelberg., 1967.

Lukens, C. E., Riebe, C. S., Sklar, L. S., and Shuster, D. L.: Grain size bias in cosmogenic nuclide studies of stream sediment in steep terrain, J. Geophys. Res. Earth Surf., 121(5), 978–999, doi:10.1002/2016JF003859, 2016.

Lupker, M., Blard, P.-H., Lavé, J., France-Lanord, C., Leanni, L., Puchol, N., Charreau, J., and Bourlès, D. L.: 10Be-derived

https://doi.org/10.5194/esurf-2019-37
Preprint. Discussion started: 1 August 2019
© Author(s) 2019. CC BY 4.0 License.



Himalayan denudation rates and sediment budgets in the Ganga basin, Earth Planet. Sci. Lett., 333–334, 146–156, doi:10.1016/j.epsl.2012.04.020, 2012.

Marshall, J. A., Roering, J. J., Gavin, D. G., and Granger, D. E.: Late Quaternary climatic controls on erosion rates and geomorphic processes in western Oregon, USA, Geol. Soc. Am. Bull., 129(5–6), 715–731, doi:10.1130/B31509.1, 2017.

Martin, L., Blard, P.-H., Balco, G., Lavé, J., Delunel, R., Lifton, N., and Laurent, V.: The CREp program and the ICE-D production rate calibration database: A fully parameterizable and updated online tool to compute cosmic-ray exposure ages, Quat. Geochronol., 38, 25–49, doi:10.1016/j.quageo.2016.11.006, 2017.

Matmon, A., Bierman, P. R., Larsen, J., Southworth, S., Pavich, M., Finkel, R. C., and Caffee, M. W.: Erosion of an Ancient Mountain Range, The Great Smoky Mountains, North Carolina and Tennessee, Am. J. Sci., 303(9), 817–855, doi:10.2475/ajs.303.9.817, 2003.

Molliex, S., Rabineau, M., Leroux, E., Bourlès, D. L., Authemayou, C., Aslanian, D., Chauvet, F., Civet, F., and Jouet, G.: Multi-approach quantification of denudation rates in the Gulf of Lion source-to-sink system (SE France), Earth Planet. Sci. Lett., 444, 101–115, doi:10.1016/j.epsl.2016.03.043, 2016.

Molnar, P.: Late Cenozoic increase in accumilation rates : How Might Climate Change Have Affected Erosion Rates?, Annu. Rev. Earth Planet. Sci., 32(1), 67–89, doi:10.1146/annurev.earth.32.091003.143456, 2004.

Montgomery, D. R.: Soil erosion and agricultural sustainability, Proc. Natl. Acad. Sci., 104(33), 13268–13272, doi:10.1073/pnas.0611508104, 2007.

Montgomery, D. R. and Brandon, M. T.: Topographic controls on erosion rates in tectonically active mountain ranges, Earth Planet. Sci. Lett., 201(3–4), 481–489, doi:10.1016/S0012-821X(02)00725-2, 2002.

Mulder, T., Savoye, B., Syvitski, J. P. M., and Parize, O.: Des courants de turbidité hyperpycnaux dans la tête du canyon du Var ? Données hydrologiques et observations de terrain, Oceanol. Acta, 20(4), 607–626, 1996.

Neilson, T. B., Schmidt, A. H., Bierman, P. R., Rood, D. H., and Sosa Gonzalez, V.: Efficacy of in situ and meteoric 10 Be mixing in fluvial sediment collected from small catchments in China, Chem. Geol., 471(June), 119–130, doi:10.1016/j.chemgeo.2017.09.024, 2017.

Niemi, N. A., Oskin, M., Burbank, D. W., Heimsath, A. M., and Gabet, E. J.: Effects of bedrock landslides on cosmogenically determined erosion rates, Earth Planet. Sci. Lett., 237(3–4), 480–498, doi:10.1016/j.epsl.2005.07.009, 2005.

Nishiizumi, K., Winterer, E. L., Kohl, C. P., Klein, J., Middleton, R., Lal, D. and Arnold, J. R.: Cosmic ray production rates of 10 Be and 26 Al in quartz from glacially polished rocks, J. Geophys. Res., 94(B12), 17907, doi:10.1029/JB094iB12p17907, 1989.

Norton, K. P., von Blanckenburg, F., Schlunegger, F., Schwab, M., and Kubik, P. W.: Cosmogenic nuclide-based investigation of spatial erosion and hillslope channel coupling in the transient foreland of the Swiss Alps, Geomorphology, 95(3–4), 474–486, doi:10.1016/j.geomorph.2007.07.013, 2008.

Norton, K. P., von Blanckenburg, F., and Kubik, P. W.: Cosmogenic nuclide-derived rates of diffusive and episodic erosion in the glacially sculpted upper Rhone Valley, Swiss Alps, Earth Surf. Process. Landforms, 35(6), n/a-n/a, doi:10.1002/esp.1961, 2010.

Norton, K. P., von Blanckenburg, F., DiBiase, R., Schlunegger, F., and Kubik, P. W.: Cosmogenic 10Be-derived denudation rates of the Eastern and Southern European Alps, Int. J. Earth Sci., 100(5), 1163–1179, doi:10.1007/s00531-010-0626-y, 2011.

Ouimet, W. B., Whipple, K. X., and Granger, D. E.: Beyond threshold hillslopes: Channel adjustment to base-level fall in tectonically active mountain ranges, Geology, 37(7), 579–582, doi:10.1130/G30013A.1, 2009.

Peizhen, Z., Molnar, P., and Downs, W. R.: Increased sedimentation rates and grain sizes 2–4 Myr ago due to the influence of climate change on erosion rates, Nature, 410(6831), 891–897, doi:10.1038/35073504, 2001.

Portenga, E. W. and Bierman, P. R.: Understanding earth's eroding surface with 10Be, GSA Today, 21(8), 4–10,

https://doi.org/10.5194/esurf-2019-37
Preprint. Discussion started: 1 August 2019
© Author(s) 2019. CC BY 4.0 License.



doi:10.1130/G111A.1, 2011.

Portenga, E. W., Bierman, P. R., Duncan, C., Corbett, L. B., Kehrwald, N. M., and Rood, D. H.: Erosion rates of the Bhutanese Himalaya determined using in situ-produced 10Be, Geomorphology, 233, 112–126, doi:10.1016/j.geomorph.2014.09.027, 2015.

Puchol, N., Lavé, J., Lupker, M., Blard, P.-H., Gallo, F., and France-Lanord, C.: Grain-size dependent concentration of cosmogenic 10Be and erosion dynamics in a landslide-dominated Himalayan watershed, Geomorphology, 224, 55–68, doi:10.1016/j.geomorph.2014.06.019, 2014.

Puchol, N., Charreau, J., Blard, P.-H., Lavé, J., Dominguez, S., Pik, R., Saint-Carlier, D., and Team, A.: Limited impact of Quaternary glaciations on denudation rates in Central Asia, Geol. Soc. Am. Bull., B31475.1, doi:10.1130/B31475.1, 2016.

Roering, J. J., Kirchner, J. W., and Dietrich, W. E.: Evidence for nonlinear, diffusive sediment transport on hillslopes and implications for landscape morphology, Water Resour. Res., 35(3), 853–870, doi:10.1029/1998WR900090, 1999.

Roering, J. J., Kirchner, J. W., and Dietrich, W. E.: Hillslope evolution by nonlinear, slope-dependent transport: Steady state morphology and equilibrium adjustment timescales, J. Geophys. Res. Solid Earth, 106(B8), 16499–16513, doi:10.1029/2001JB000323, 2001.

Roure, J., Autran, A., Prost, A., Rossi, A., and Rousset, C.: Carte géologique de la France à 1/250 000 - Nice, 1976.

Savi, S., Norton, K. P., Picotti, V., Brardinoni, F., Akçar, N., Kubik, P. W., Delunel, R., and Schlunegger, F.: Effects of sediment mixing on 10Be concentrations in the Zielbach catchment, central-eastern Italian Alps, Quat. Geochronol., 19, 148–162, doi:10.1016/j.quageo.2013.01.006, 2014.

Schaller, M., von Blanckenburg, F., Veldkamp, A., Tebbens, L. A., Hovius, N., and Kubik, P. W.: A 30 000 yr record of erosion rates from cosmogenic 10Be in Middle European river terraces, Earth Planet. Sci. Lett., 204(1–2), 307–320, doi:10.1016/S0012-821X(02)00951-2, 2002.

Sosa Gonzalez, V., Schmidt, A. H., Bierman, P. R., and Rood, D. H.: Spatial and temporal replicability of meteoric and in situ 10 Be concentrations in fluvial sediment, Earth Surf. Process. Landforms, 42(15), 2570–2584, doi:10.1002/esp.4205, 2017.

Stockmann, U., Minasny, B. and McBratney, A. B.: How fast does soil grow?, Geoderma, 216, 48–61, doi:10.1016/j.geoderma.2013.10.007, 2014.

Stone, J. O. H.: Air pressure and cosmogenic isotope production, J. Geophys. Res. Solid Earth, 105(B10), 23753–23759, doi:10.1029/2000JB900181, 2000.

Wittmann, H., von Blanckenburg, F., Kruesmann, T., Norton, K. P., and Kubik, P. W.: Relation between rock uplift and denudation from cosmogenic nuclides in river sediment in the Central Alps of Switzerland, J. Geophys. Res., 112(F4), F04010, doi:10.1029/2006JF000729, 2007.

Wittmann, H., Malusà, M. G., Resentini, A., Garzanti, E., and Niedermann, S.: The cosmogenic record of mountain erosion transmitted across a foreland basin: Source-to-sink analysis of in situ 10Be, 26Al and 21Ne in sediment of the Po river catchment, Earth Planet. Sci. Lett., 452, 258–271, doi:10.1016/j.epsl.2016.07.017, 2016.

Yanites, B. J. and Ehlers, T. A.: Global climate and tectonic controls on the denudation of glaciated mountains., 2012.

Yanites, B. J., Tucker, G. E., and Anderson, R. S.: Numerical and analytical models of cosmogenic radionuclide dynamics in landslide-dominated drainage basins, J. Geophys. Res., 114(F1), F01007, doi:10.1029/2008JF001088, 2009.

Yu, F., Hunt, A., Egli, M., and Raab, G.: Comparison and contrast in soil depth evolution for steady-state and stochastic erosion processes: Possible implications for landslide prediction, Geochemistry, Geophys. Geosystems, 2018GC008125, doi:10.1029/2018GC008125, 2019.

https://doi.org/10.5194/esurf-2019-37
Preprint. Discussion started: 1 August 2019
© Author(s) 2019. CC BY 4.0 License.

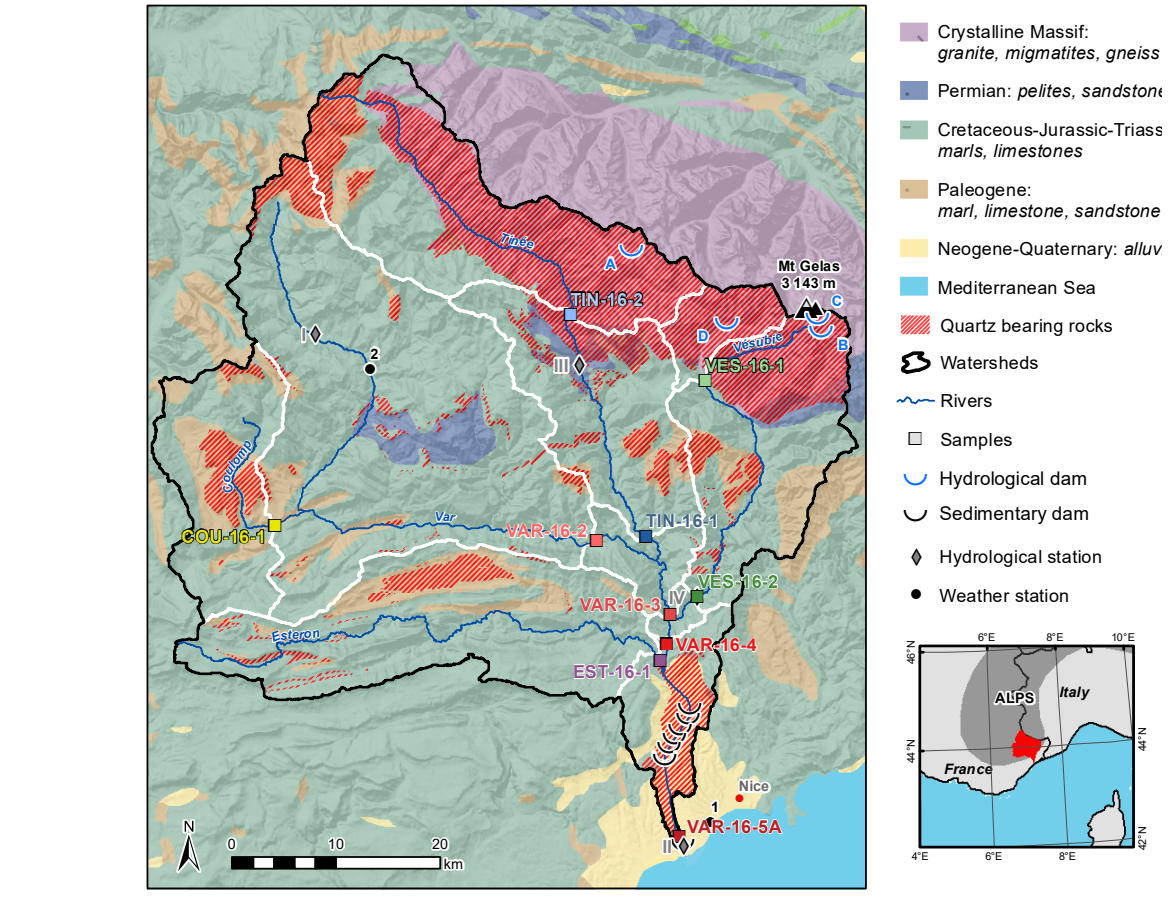


Figure 1: Geological setting of the Var basin and its subbasins. Geological data are from the French Geological Survey (see text for references). White lines delimit the sampled subbasins, colored squares represent sampling points and red hashed areas indicate the presence of quartz-bearing rocks. Hydrological station data are from the HYDRO database (www.hydro.eaufrance.fr): I, Villneuve d'Entraunes station; II, Nice, Pont Napoléon station; III, Saint Sauveur sur Tinée station; and IV, Utelle station. Hydrological dams are: A, Isloa 2000 dam; B, Lac Fous dam; C, Lac Long dam; and D, Lac Boréon dam. Weather stations are from Météo France: 1, Nice; and 2, Guillaumes. The outset maps indicates the location of the Var basin in the southern French Alps.

https://doi.org/10.5194/esurf-2019-37
Preprint. Discussion started: 1 August 2019
© Author(s) 2019. CC BY 4.0 License.



Earth Surface Dynamics Discussions
Open Access
EGU

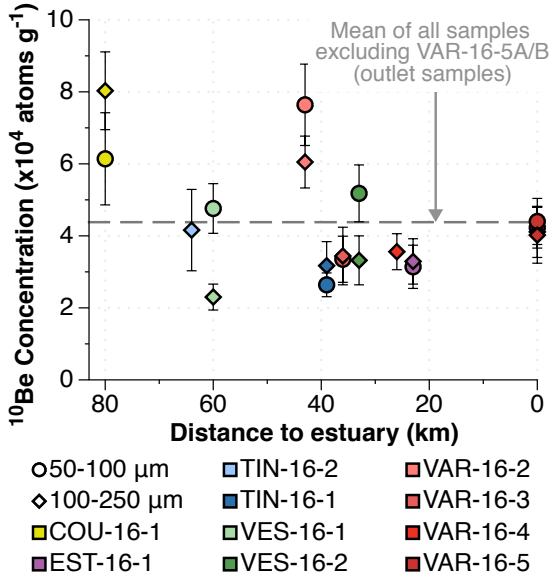


Figure 2: ^{10}Be concentrations in quartz from river sands of the Var basin plotted against the distance to the estuary (km). Data are available in Table 1. Symbol shape reflects the analyzed grain size and colors indicate the subbasin. The dashed line corresponds to the mean concentration of all samples, excluding the four outlet samples. Error bars represent 1 sigma uncertainties.

https://doi.org/10.5194/esurf-2019-37
Preprint. Discussion started: 1 August 2019
© Author(s) 2019. CC BY 4.0 License.

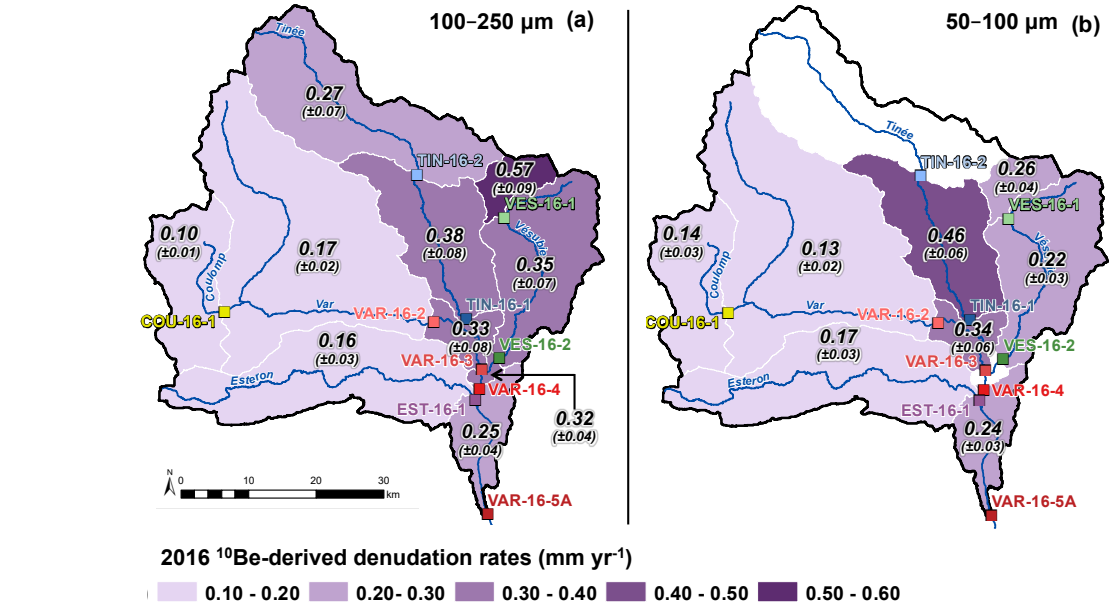


Figure 3: Spatial variations of ^{10}Be-derived denudation rates for the 2016 Var samples (data reported in Table 1). White polygons denote the absence of data. Denudation rates were derived from the (a) 100–250 µm and (b) 50–100 µm grain size fractions.

https://doi.org/10.5194/esurf-2019-37
Preprint. Discussion started: 1 August 2019
© Author(s) 2019. CC BY 4.0 License.

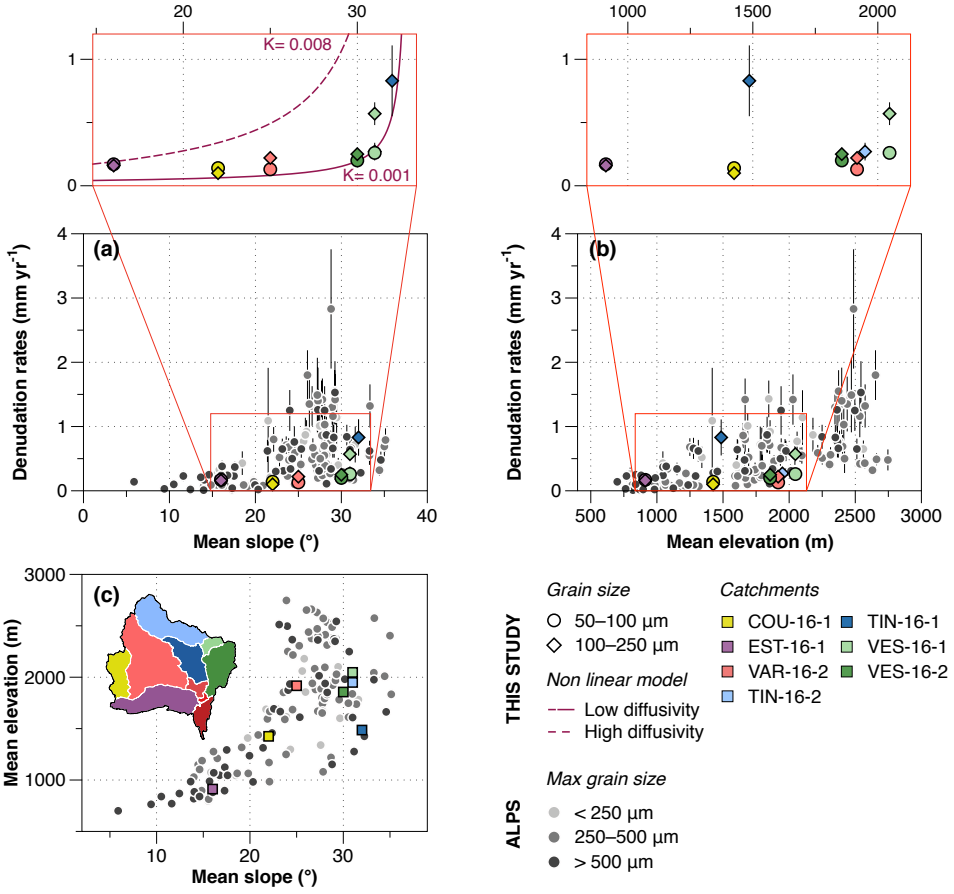


Figure 4: ^{10}Be derived denudation rates in the Var basin and elsewhere in the Alps plotted against (a) mean basin slope and (b) mean basin elevation. The relationship between mean elevation and slope is plotted in (c). For the Var basin, all parameters were calculated for quartz-bearing surfaces only using a 5 m resolution DEM from the Institut National de l'Information Géographique et Forestière (http://professionnels.ign.fr/donnees). For the COU-16-1, EST-16-1, TIN-16-2 and VES-16-1 subbasins, we used denudation rates from Table 1. For the VAR-16-2, TIN-16-1 and VES-16-2 subbasins, we used subbasin ^{10}Be denudation rates (Table 2) to exclude their nested upstream subbasins (COU-16-1, TIN-16-2 and VES-16-1, respectively). We used the OCTOPUS database (Codilean et al., 2018) to acquire data from the Alps (Buechi et al., 2014; Chittenden et al., 2014; Delunel et al., 2010; Dixon et al., 2016; Glotzbach et al., 2013; Grischott et al., 2016; Molliex et al., 2016; Norton et al., 2008, 2010, 2011; Savi et al., 2014; Wittmann et al., 2007, 2016). The nonlinear denudation model is from Montgomery and Brandon (2002) using a chemical weathering rate of 0.023 mm yr^{-1} for the Var (the mean value between spring and winter from Donnini et al., 2016), a critical slope of 33° (similar to Ouimet et al., 2009) and diffusivities (K) of 0.001 m yr^{-1} and 0.008 m yr^{-1}, which are within the range of global values complied by Hurst et al. (2013).

https://doi.org/10.5194/esurf-2019-37
Preprint. Discussion started: 1 August 2019
© Author(s) 2019. CC BY 4.0 License.

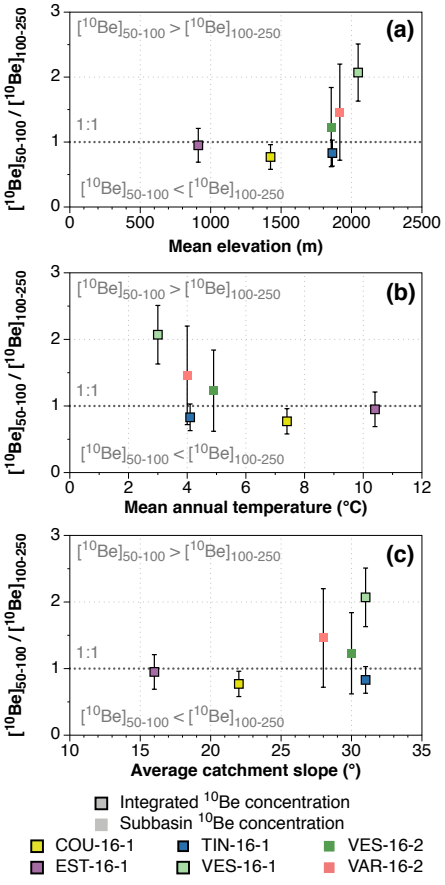


Figure 5: Differences in ^{10}Be concentrations of the 50–100 and 100–250 µm size fractions as a function of (a) elevation, (b) mean annual temperature and (c) average subbasin slope. Mean elevation and temperature were calculated for quartz-bearing surfaces only using a 5 m resolution DEM from the Institut National de l'Information Géographique et Forestière (http://professionnels.ign.fr/donnees). Temperature data are from the WorldClim database (http://worldclim.org/version2; Fick and Hijmans, 2017). Subbasin concentrations (Table 2) are used for VES-16-2 and VAR-16-2 to exclude their nested upstream subbasins (VES-16-1 and COU-16-1, respectively).

https://doi.org/10.5194/esurf-2019-37
Preprint. Discussion started: 1 August 2019
© Author(s) 2019. CC BY 4.0 License.



Earth Surface Dynamics Discussions
Open Access
EGU

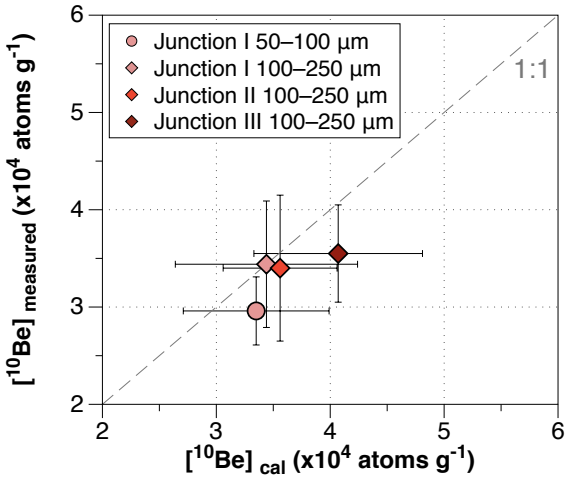


Figure 6: ^{10}Be concentrations of sediments at three river junctions calculated using Eq. (2) plotted against those measured in sediments downstream of the tributary junctions (Table 1). Junction I is the Var-Tinée junction, measured at VAR-16-3; Junction II is the Var-Vésubie junction, measured at VAR-16-4; and Junction III is the Var-Estéron junction, measured at VAR-16-5A/B. For Junction III, the measured concentration is the average of the concentrations in the 100–250 µm size fractions at VAR-16-5A and VAR-16-5B.

https://doi.org/10.5194/esurf-2019-37
Preprint. Discussion started: 1 August 2019
© Author(s) 2019. CC BY 4.0 License.

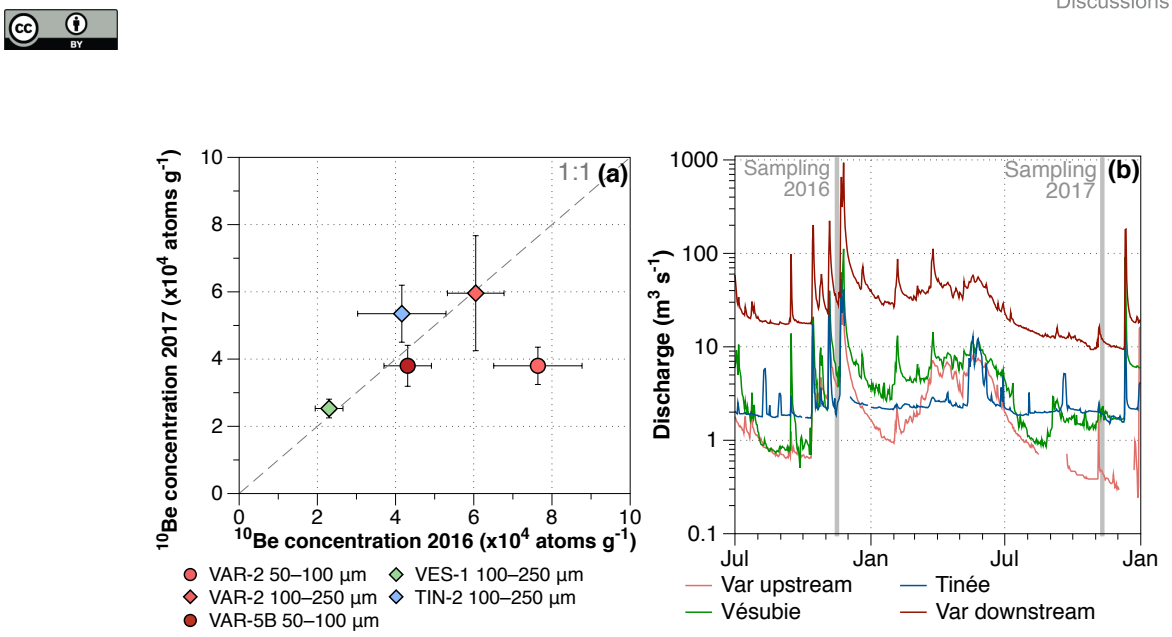


Figure 7: Interannual variability of sediment ^{10}Be concentrations. (a) Concentrations in sediments sampled in 2016 (x axis) are plotted against sediments of the same size fraction sampled in the same locations in 2017 (y axis). Most samples are in agreement with the 1:1 line, indicating little interannual variation. Only the 50–100 µm fraction at VAR-2 does not show the same trend. (b) Daily discharge data (log scale) from four hydrological stations in the Var basin (see Fig. 1): Var upstream (station I, Villneuve d'Entraunes), Vésubie (station IV, Utelle), Tinée (station III, Saint Sauveur sur Tinée) and Var downstream (station II, Nice, Pont Napoléon). Discharge data are freely accessible at www.hydro.eaufrance.fr.

https://doi.org/10.5194/esurf-2019-37
Preprint. Discussion started: 1 August 2019
© Author(s) 2019. CC BY 4.0 License.



Earth Surface Dynamics Discussions
Open Access
EGU

River	Sample Name	Grain size	Lat.	Long.	Quartz-bearing area	Mass quartz	**^{10}Be concentration**	**1 sigma, ^{10}Be concentration**	Neutron production rate	Fast muon prod rate	Slow muon prod rate	**Denudation rate**	**1 sigma, denudation rate**	Integration time
		µm	°N	°E	km^2	g	**at g^{-1}**	**at g^{-1}**	at g^{-1} yr^{-1}	at g^{-1} yr^{-1}	at g^{-1} yr^{-1}	**mm yr^{-1}**	**mm yr^{-1}**	yr
2016														
Coulomp	COU-16-1	50–100	43.959	6.730	36.1	2.9	**6.14 ×10^4**	**1.28 ×10^4**	12.506	0.049	0.021	**0.14**	**0.03**	4430
		100–250				27.9	**8.03 ×10^4**	**1.08 ×10^4**	12.644			**0.10**	**0.01**	5732
Esteron	EST-16-1	50–100	43.825	7.183	39.1	19.3	**3.14 ×10^4**	**6.04 ×10^3**	7.727	0.044	0.016	**0.17**	**0.03**	3505
		100–250				6.2	**3.29 ×10^4**	**6.30 ×10^3**	7.727			**0.16**	**0.03**	3677
Tinée	TIN-16-2	100–250	44.128	7.097	293.6	3.7	**4.16 ×10^4**	**1.13 ×10^4**	17.458	0.055	0.026	**0.27**	**0.07**	2197
	TIN-16-1	50–100	43.933	7.717	365.1	27.9	**2.64 ×10^4**	**3.34 ×10^3**	18.714	0.054	0.025	**0.46**	**0.06**	1310
		100–250				16.6	**3.17 ×10^4**	**6.67 ×10^3**	18.714			**0.38**	**0.08**	1573
Var	VAR-16-2	50–100	43.931	7.115	83.8	7.1	**7.64 ×10^4**	**1.13 ×10^4**	15.699	0.052	0.023	**0.13**	**0.02**	4463
		100–250				12.7	**6.05 ×10^4**	**7.24 ×10^3**	15.699			**0.17**	**0.02**	3534
	VAR-16-3	50–100	43.865	7.198	449.3	6.4	**3.35 ×10^4**	**6.36 ×10^3**	17.315	0.053	0.024	**0.34**	**0.06**	1785
		100–250				14.6	**3.44 ×10^4**	**7.99 ×10^3**	17.315			**0.33**	**0.08**	1834
	VAR-16-4	100–250	43.839	7.192	633.3	8.4	**3.56 ×10^4**	**4.98 ×10^3**	17.356	0.054	0.025	**0.32**	**0.04**	1892
	VAR-16-5A	50–100	43.672	7.166	730.3	27.0	**4.40 ×10^4**	**6.42 ×10^3**	15.593	0.052	0.023	**0.23**	**0.03**	2587
		100–250				13.0	**4.02 ×10^4**	**7.82 ×10^3**	15.765			**0.26**	**0.05**	2344
	VAR-16-5B	50–100	43.672	7.195		5.5	**4.23 ×10^4**	**5.72 ×10^3**	15.593			**0.24**	**0.03**	2489
		100–250				4.9	**4.11 ×10^4**	**7.04 ×10^3**	15.765			**0.25**	**0.04**	2395
Vésubie	VES-16-1	50–100	44.065	7.255	59.4	22.6	**4.76 ×10^4**	**6.91 ×10^3**	19.479	0.056	0.026	**0.26**	**0.04**	2270
		100–250				33.2	**2.30 ×10^4**	**3.55 ×10^3**	20.326			**0.57**	**0.09**	1054
	VES-16-2	50–100	43.879	7.231	184.0	32.8	**5.18 ×10^4**	**7.89 ×10^3**	17.892	0.054	0.025	**0.22**	**0.03**	2731
		100–250				29.2	**3.32 ×10^4**	**6.84 ×10^3**	17.892			**0.35**	**0.07**	1714
2017														
Tinée	TIN-17-2	100-250	44.128	7.097	293.6	13.1	**5.35 ×10^4**	**8.48 ×10^3**	17.269	0.055	0.026	**0.21**	**0.03**	2853
Var	VAR-17-2	50–100	43.931	7.115	83.8	7.0	**3.80 ×10^4**	**5.55 ×10^3**	16.044	0.052	0.023	**0.34**	**0.06**	1766
		100–250				14.7	**5.96 ×10^4**	**1.71 ×10^4**	15.699			**0.17**	**0.05**	3479
	VAR-17-5B	50–100	43.672	7.195	730.3	10.5	**3.80 ×10^4**	**6.09 ×10^3**	15.765	0.052	0.023	**0.27**	**0.04**	2216
Vésubie	VES-17-1	100–250	44.065	7.255	59.4	61.1	**2.53 ×10^4**	**2.78 ×10^3**	20.326	0.056	0.026	**0.52**	**0.06**	1161

Table 1: ^{10}Be-derived denudation rates in the Var basin in 2016 and 2017. Reported ^{10}Be concentrations have been corrected for analytical blanks (Raw data available in Supplementary materials). ^{10}Be/^{9}Be ratios were calibrated using the CEREGE STD11 in-house normalization (Braucher et al., 2015). Neutron production rates include paleomagnetic modulations over the integration time. Denudation rates were calculated with neutron, fast muon and slow muon attenuation lengths 160 g cm^{-2}, 4320 g cm^{-2} and 1500 g cm^{-2}, respectively (Braucher et al., 2011), and assuming a rock density of 2.7 g cm^{-3}. Integration time represents the time required to remove 60 cm of bedrock.

https://doi.org/10.5194/esurf-2019-37
Preprint. Discussion started: 1 August 2019
© Author(s) 2019. CC BY 4.0 License.



Earth Surface Dynamics Discussions
Open Access
EGU

River	Name	Grain size	Quartz-bearing area	Subbasin ^{10}Be concentration	Subbasin 1 sigma, ^{10}Be concentration	Subbasin Denudation rate	Subbasin 1 sigma, denudation rate	Subbasin Integration time
		µm	km^2	at g^{-1}	at g^{-1}	mm yr^{-1}	mm yr^{-1}	kyr
Tinée	TIN-16-1	100–250	71.5	**1.82×10^4**	**1.01×10^4**	**0.83**	**0.28**	0.7
Var	VAR-16-2	50–100	47.7	**7.77×10^4**	**3.24×10^4**	**0.13**	**0.03**	4.5
		100–250		**5.33×10^4**	**1.54×10^4**	**0.22**	**0.04**	2.7
Vésubie	VES-16-2	50–100	124.6	**5.45×10^4**	**1.80×10^4**	**0.20**	**0.04**	3.0
		100–250		**4.44×10^4**	**1.63×10^4**	**0.25**	**0.05**	2.4

Table 2: Subbasin ^{10}Be concentrations and denudation rates in the Var basin in 2016. These effective denudation rates were calculated by excluding nested upstream subbasins following the method of Portenga et al. (2015). Denudation rates were calculated with neutron, fast muon and slow muon attenuation lengths of 160 g cm^{-2}, 4320 g cm^{-2} and 1500 g cm^{-2}, respectively (Braucher et al., 2011), and assuming a rock density of 2.7 g cm^{-3}. Integration time represents the time required to remove 60 cm of bedrock.